Dalton Transactions

Accepted Manuscript

ROYAL SOCIETY OF CHEMISTRY

www.rsc.org/dalton

Journal Name

ARTICLE

Highly Selective and Sensitive Fluorescence Detection of Zn^{2+} and Cd^{2+} Ions by an Acridine Sensor

Received 00th January 20xx,
Accepted 00th January 20xx

DOI: 10.1039/x0xx00000x

www.rsc.org/

A. Visscher,[a] S. Bachmann,[a] C. Schnegelsberg,[b] T. Teuteberg,[c] R. Mata[c] and D. Stalke*[a]

Fluorescence spectroscopic investigations of the new acridine derivative bis(*N*,*N*-dimethyl-aminemethylene)acridine (**3**) show remarkable selectivity and sensitivity towards Zn^{2+} and Cd^{2+} ions in methanol and for the latter even in water. Through the chelation of the metal ions the present PET effect is quenched, significantly enhancing the emission intensity of the fluorophore. In solution, the bonding situation is studied by fluorescence and NMR spectroscopy, as well as ESI-TOF mass-spectrometry measurements. The solid state environment is investigated by X-ray diffraction and computational calculations. Here, we can show the complexation of the zinc and cadmium ions by the methylene bridged amine receptors as well as by the nitrogen atom of the acridine system. To our knowledge, this coordination motif is unprecedented in fluorescent sensor chemistry.

Introduction

The detection of metal ions in solution has always been an important topic in analytical chemistry, environmental protection and medicinal applications. Metal ions like magnesium, calcium, or zinc are essential components of many enzymes in the human body.[1] Especially Zn^{2+} plays a prescind role in many different areas; e.g. in the emergence of Alzheimer's disease.[2] Moreover, its level of concentration could help to diagnose the growing of tumour cells in the prostate.[3] Zinc deficiency increases the susceptibility to a variety of pathogens and is of central importance for the immune system.[4]

The heavier homologue Cd^{2+} is known to be a very toxic metal ion. Over several decades in the first half of the 20th century, hundreds of people in Japan were affected by the deadly *itai-itai* disease due to a cadmium polluted river.[5] Therefore, it is vital to have a fast working and very sensitive method for the detection of metal ions in e.g. blood or water supplies. Fluorescence spectroscopy combined with suitable fluorescent sensors is a well-recognized method for such analysis. Sensor molecules should be able to switch instantaneously between a fluorescent on/off state or change their emission wavelength significantly upon addition of an analyte. To achieve this response several different mechanisms can be employed. Besides intramolecular charge transfer (ICT),[6] metal-ligand charge transfer (MLCT)[7] or excimer formation,[8] an extensively investigated concept is the photoinduced electron transfer (PET)[9] effect. Here a poor or non-fluorescent ligand starts to emit light upon coordination of an analyte under UV light irradiation.

The great interest in molecular sensors is reflected by the multitude of publications.[10] Acridine derivatives in particular are commonly applied in the detection of bioorganic compounds. For example it is frequently used as a fluorescence dye for DNA intercalation.[11] Acridine based sensors for cationic analytes are less commonly used[12] since they often do not show a strong enhancement of the fluorescence emssion.[13] In the following, we present the characterization in the solid state and in solution of an interesting new acridine based sensor.

Results and Discussion

Synthesis

Many of the molecular sensors reported in literature contain elaborated side arms working as the receptor unit.[10a, 14] However, another requirement to be met by a sensor is the economic aspect of feasible and cheap availability. Therefore, we chose a short and effective synthetic route to produce derivatives of acridine systems with small amine side arms (Scheme 1). The desired sensor system with the concept "fluorophore-spacer-receptor" can be obtained in a quick two-step synthesis. The two bromomethylene units can easily be

[a] *Institut für Anorganische Chemie der Universität Göttingen, Tammannstraße 4, 37077 Göttingen, Germany. E-mail: dstalke@chemie.uni-goettingen.de*
[b] *Institut für Organische und Biomolekulare Chemie der Universität Göttingen, Tammannstraße 2, 37077 Göttingen, Germany.*
[c] *Institut für Physikalische Chemie der Universität Göttingen, Tammannstraße 6, 37077 Göttingen, Germany.*
Electronic Supplementary Information (ESI) available: Further spectroscopic data like NMR, UV/vis, fluorescence, and mass spectra as well as crystallographic and computational tables. See DOI: 10.1039/x0xx00000x

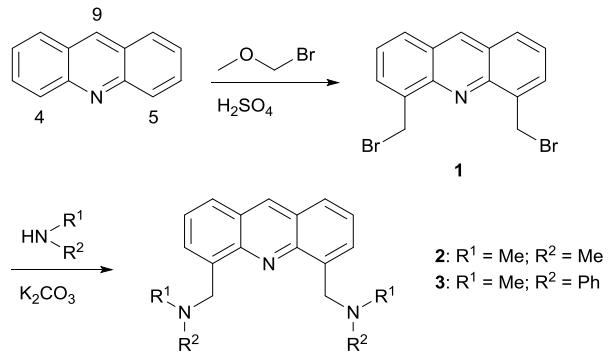

Scheme 1: Reaction pathway to 4,5-substituted acridine derivatives.

introduced in the 4- and 5-position through bromomethyl methyl ether (BMME) functions and a strong acid like conc. H_2SO_4.[15] The bromine atoms can straightforwardly be substituted by a variety of amines. In this publication we present two new acridine derivatives with distinct amine moieties: 4,5-bis(*N*-methyl-*N*-phenylaminemethylene)acridine (**2**) and 4,5-bis(*N*,*N*-dimethylaminemethylene)acridine (**3**). Although the two molecules are very similar only the latter shows extraordinary fluorescence properties.

The introduction of two receptor units directly neighboured to the aromatic nitrogen atom holds the option to coordinate a target cation with the side arms as well as with the fluorophore. This is a great advantage compared to its lighter congener, the widely used fluorophore anthracene.[13, 14b]

Fluorescence Studies

The fluorescence measurements were carried out in methanol in which both the ligands and the metal salts are readily soluble. Moreover, this protic and very polar solvent exhibits similar properties to water, which is important for possible future applications. The employed structural design (fluorophore-spacer-receptor) results in a very efficient electron transfer which is favourable for a molecular off/on switch: The methylene units (spacer) allow the amines (receptor) to rotate easily about their N–C and C–C bonds. This provides the conformational freedom to interact electronically with the π-system of the acridine (fluorophore) and results in an effective quenching of the fluorescence.[16] At the same time the amines are able to employ their lone pair in complexation of analytes. If this is the case, the PET is hindered and the emission of light is facilitated. Figure 1 shows the excitation and emission spectra of the ligands **2** and **3** in methanol.

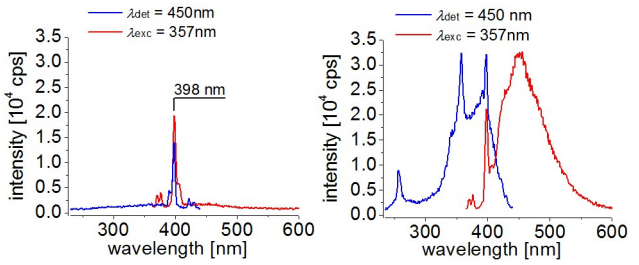

Figure 1: Excitation (blue, λ_{det} = 450 nm) and emission spectra (red, λ_{exc} = 357 nm) of **2** (left) and **3** (right) in a 10^{-5} M methanol solution.

The emission intensities of both ligands are very weak, whereas they show a strong absorption behaviour (SI Figure S4.1) which hints at a working PET. Interestingly, the intensity of the methyl derivative **3** is considerably higher than the phenyl derivative **2**. This observation could indicate impurities and will be discussed later in full detail. In Figure 1, left, the highest peak at 398 nm in both spectra is attributed to Raman scattering of the used solvent methanol.[17]

In a next step, a metal ion screening was conducted to check the sensing ability of the ligands. Here sixteen different metal salts were dissolved in methanol and each was titrated to the $1{\cdot}10^{-5}$ M concentrated solutions of the ligands, respectively. To afford a good comparability, the metal ion concentrations were increased stepwise in the same manner (1, 5, 15, 100 eq). Additionally, only bromides were used to standardize possible interference of the counter ion. With **2** as ligand system, no significant change in emission intensity is observed for the tested metal salts (SI Figure S5.1). To check whether the structural motif nevertheless is suitable as a sensor in general, we used the less polar and donating solvent dichloromethane. In this solution we observed a massive fluorescence enhancement by adding $ZnBr_2$ to the ligand (SI Figure S5.2). Since this solvent is not in the focus of our interest, we concentrated on the dimethylamine system **3**. In Figure 2, we compare the intensity maxima of its emission spectra during the metal ion screening. Among the tested sixteen metal salts this ligand shows a very high selectivity towards Zn^{2+} and Cd^{2+} ions. The emission intensity increases enormously. The only minute emission enhancement with $AlBr_3$ and $SnBr_2$ is solely due to the strong Lewis acidity of these metal ions which leads to slight protonation of the ligand. This can be evidenced by the different resulting emission wavelengths. If the ligand is protonated, the wavelength of the emission maximum is blue-shifted to 425 nm (SI Figure S5.4), whereas in the case of Zn^{2+} or Cd^{2+} coordination the maximum is observed at 457 nm and 445 nm, respectively. In this context it should be mentioned that although the emission shift between the two metal ions is only 12 nm this is sufficient to differentiate the metals by fluorescence spectroscopy. A closer look at the detailed emission spectra depicted in Figure 3 additionally demonstrates the high sensitivity of this sensor molecule.

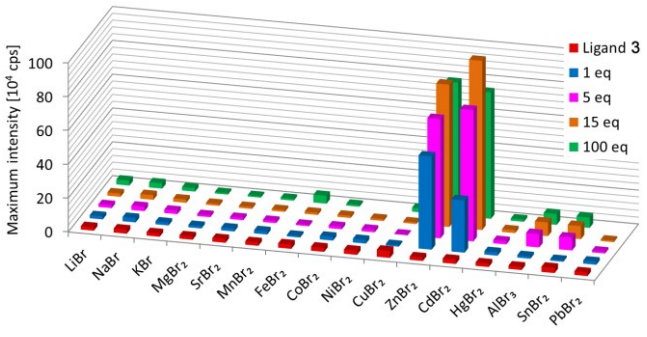

Figure 2: Metal ion screening with ligand **3** in methanol (c = $1{\cdot}10^{-5}$ M). The maximum emission intensity is depicted for each metal ion addition (λ_{exc} = 357 nm).

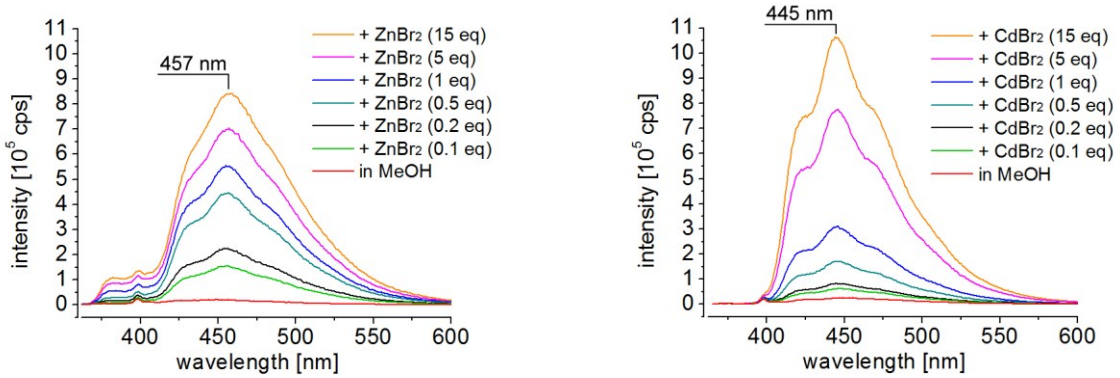

Figure 3: Emission spectra of **3** titrated with $ZnBr_2$ (left) and $CdBr_2$ (right) in methanol; both were irradiated at 357 nm.

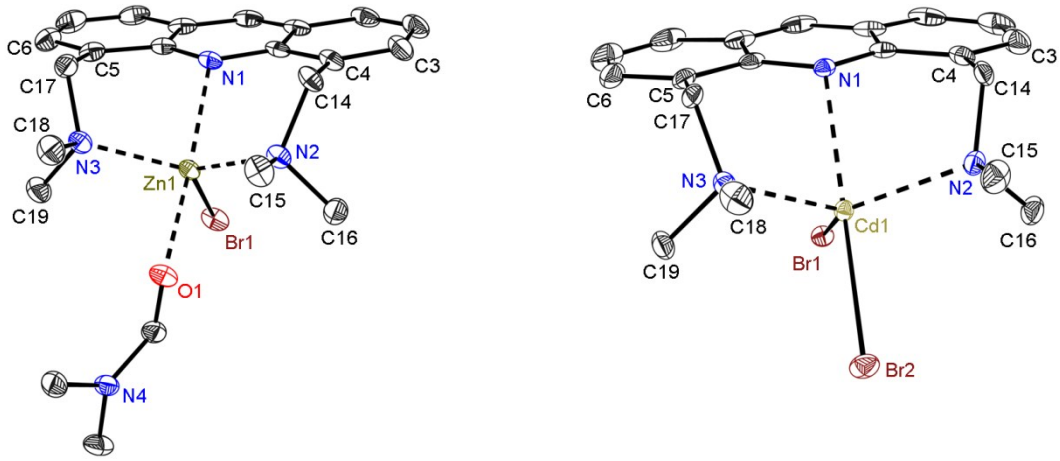

Figure 4: Solid state structures of $[(dmf)ZnBr\{(Me_2NCH_2)_2Acr\}]^+$ (**4a**, left) and $[CdBr_2\{(Me_2NCH_2)_2Acr\}]$ (**5**, right); crystallized from a THF/DMF mixture. The omitted counter anion in the asymmetric unit of the zinc structure is a solvent-separated $[(dmf)ZnBr_3]^-$ unit. All hydrogen atoms were omitted for clarity. Anisotropic displacement parameters are depicted at the 50% probability level.

Table 1: Selected bond lengths [pm] and angles [°]. The angular sums arise from the C–N–C angles.

Bond [pm]	**4a** (Zn)	**5** (Cd)	Angle [°]	**4a** (Zn)	**5** (Cd)
N1–M	230.39(16)	254.07(18)	N1–M–N2	90.05(6)	82.91(6)
N2–M	207.89(16)	232.31(19)	N1–M–N3	89.81(6)	82.81(6)
N3–M	209.09(17)	231.70(19)	N2–M–N3	128.68(6)	120.87(7)
Br1–M	239.83(4)	259.13(4)	N1–M–O1/Br2	175.31(6)	174.08(4)
O1/Br2–M	218.82(14)	266.16(4)	angular sum of N2	325.0(5)	327.1(6)
			angular sum of N3	324.0(5)	327.0(6)
			C3–C4–C14–N2	–114.8(2)	–105.3(3)
			C6–C5–C17–N3	112.7(2)	105.9(3)

After adding only 0.1 eq of $ZnBr_2$ to the ligand solution, a significant increase of emission intensity is observed. Besides the standard titration of the analytes, we checked the reversibility of the metal complexation. Therefore, we alternately added a specified amount of metal salt and ethylenediamine (en) to the ligand ($CdBr_2$ is depicted in Figure 5, for $ZnBr_2$ see SI Figure S5.6). With 1 eq of $CdBr_2$ in the cuvette, the emission intensity rises from 0.2 to $3.5 \cdot 10^5$ cps and is afterwards quenched to $0.1 \cdot 10^5$ cps when 10 eq of the chelating amine are added.

This experiment can be repeated several times, confirming the great reversibility of the complexation of the two metal ions. Moreover, the starting intensity of the pure ligand (red line) is about twice as high as the intensity after adding ethylenediamine. This indicates possible traces of impurities by preparing the ligand solutions. The methanol was purchased from VWR Chemicals® (AnalaR NORMAPUR) which provides analytical data for their solvents. Each kilogram contains impurities of < 0.2 mg Zn^{2+} and < 0.01 mg Cd^{2+} ions.

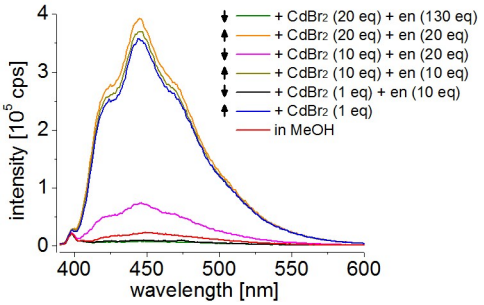

Figure 5: Reversibility of metal complexation of **3** with alternating addition of $CdBr_2$ and ethylenediamine (en); all substances are dissolved in methanol (λ_{exc} = 357 nm).

Table 2: The maximum emission intensities of the metal complexes of **3** and their relative emission intensities compared with anthracene. All measurements were done with 10^{-5} M solutions in methanol.

compound	λ_{exc} [nm]	intensity [10^4 cps]	relative intensity
3 + $ZnBr_2$	357	84.15	0.12
3 + $CdBr_2$	357	105.83	0.15
3 + $Zn(OAc)_2$	357	678.63	0.95
anthracene	373	711.91	1.00

Converted to the employed volume and concentration for the measurements, every sample could contain an amount of < 0.3 eq Zn^{2+} ions and < 0.009 eq Cd^{2+} ions with respect to the ligand. This is a significant amount one has to consider when comparing the results. But again, this underlines the sensitivity of the synthesized sensor system which enables even to detect traces of impurities. In addition, this could explain the higher excitation and emission spectrum of **3** in comparison to **2** (Figure 1), which is not sensitive to the mentioned metal ions.

In addition to the bromide salt, we investigated the influence of $Zn(OAc)_2$ and $Zn(NO_3)_2$ on the fluorescence properties of **3**. With small additions of the nitrate salt, the emission intensity rises as usual whereas an excess quickly leads to its reduction. However, using acetate as the counter anion, the fluorescence is increased strongly even resulting in an eight times higher emission maximum than with $ZnBr_2$ (SI Figure S5.5).

For a better assessment of the measured fluorescence values, the relative emission intensities are compared with the typical fluorescent compound anthracene. In Table 2, the maximum intensities of the used compounds and their relative intensities divided by the fluorescence of anthracene are shown.

Investigations of the metal complexes

To gain a better understanding of the observed fluorescence properties, it is necessary to know how the metal ions are linked to the ligand. Therefore, we synthesized the two metal complexes and investigated them with different analytical methods. For the synthesis of **4**, the ligand and $ZnBr_2$ were dissolved in THF whereas MeOH was used for the preparation of **5** (Scheme 2). In both cases, one equivalent of the metal salts was added dropwise to **3**, resulting in an immediate precipitation of the metal complexes. The crystallization of **3** with zinc acetate to give **7** was endeavoured to check whether complexes with different zinc salts behave the same which is

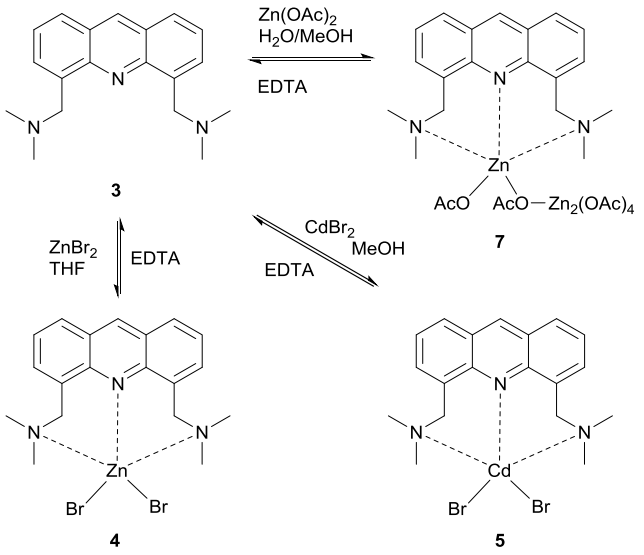

Scheme 2: Reaction pathways to the metal ion complexes **4**, **5** and **7**.

indeed the case here. The comparison of the crystal structures containing zinc ions are discussed in the SI. The single crystals of **4a** and **5** were obtained from crystallization in a THF/DMF mixture. By X-ray diffraction experiments, we could determine their solid state structures (Figure 4). The zinc complex **4a** crystallizes in the monoclinic space group $P2_1/c$ and the cadmium derivative in the chiral orthorhombic space group $P2_12_12_1$. Both complexes are almost isostructural. In the zinc structure one bromide ion is substituted by a coordinating solvent molecule DMF. The positively charged complex is counterbalanced by a solvent-separated $[ZnBr_3]^-$ anion in the asymmetric unit (SI Figure S7.1).

The solid state structures indicate a coordination of the Zn^{2+} and Cd^{2+} ions by all three present nitrogen atoms. This binding motif where the methylene bridged amines in 4- and 5-position and the aromatic nitrogen atom of the acridine all are involved in a metal ion coordination is currently not present in the CSD. Only two examples with methylene bridged phosphorous atoms coordinating a ruthenium ion can be found in the database.[18] Overall, a structural search concerning a coordination of an acridine unit to any metal ion merely results in 50 hits.[19]

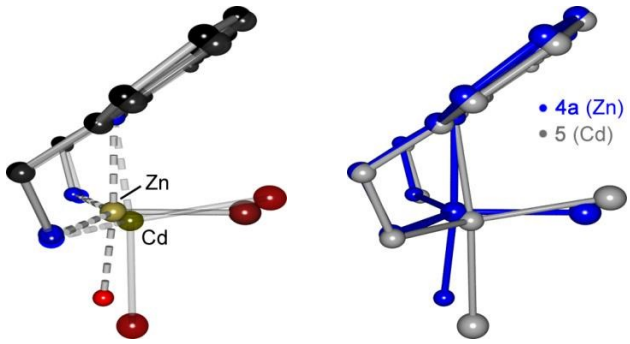

Figure 6: Superpositions of both metal ion structures (**4a**, **5**), showing the trigonal bipyramidal geometry of the coordination motif. The methyl groups at the amines and the main part of the DMF molecule are omitted for clarity.

From the nitrogen-metal bond lengths in Table 1 it is obvious that the averaged distances from the amine nitrogen atoms to the metal ion (208.49(17) for Zn^{2+} and 232.01(19) pm for Cd^{2+}) is shorter than from the acridine nitrogen atom (230.39(16) and 254.07(18) pm, respectively). The shorter distances are in perfect agreement with literature values found in the CSD, compared to general N–Zn^{2+}/Cd^{2+} bonds. The longer distances can still be found in the database quoted as bonds but less frequently. One reason for this different bonding situation results from the rotational ability of the amines to improve the orbital overlap with the target ions. The C–N–C angles of the sp^3-hybridized amines are very close to the ideal tetrahedral angle. The resulting best geometry forces the metal ion underneath the acridine plane which reduces the dative bonding to the ring nitrogen atom. Moreover, the lone pair of that sp^2-hybridized nitrogen atom is partly delocalized in the π-system of the aromatic system and has therefore a reduced donor capacity. The N–M bond incloses an relatively acute angle of 44.5 °(**4a**) and 38.5 °(**5**), to the plane of the central acridine ring. A closer look at the bonding situation and the angle values in Table 1 reveals the coordination polyhedron of a trigonal bipyramid at each metal atom. This geometry is depicted in Figure 6.

Although the longer N–M^{2+} distances can still be found in the CSD, the solid state investigations are not a sufficient evidence for the existence of a bonding situation.[20] In order to judge on the main binding forces of the metal ion coordination, and to relate the findings to the chemistry in solution, we conducted a series of electronic structure calculations on the Zn^{2+} and Cd^{2+} compounds. All structures were optimized at the B3LYP-D3/def2-TZVPP[21] level of theory. Included were the complexes **4a** and **5**, identified in the solid state structures, as well as the hypothetical complex **4**. The structures obtained are in good agreement with the crystal data (SI). A natural bond orbital (NBO) analysis[22] was carried out to gain insight into the coordination of the metals to the acridine derivative **3**. The data in Table 3 give the second order perturbation theory energies[23] for the interaction between the lone pairs of the different nitrogen atoms of **3** and the zinc or cadmium ion. As expected, in these structures the metal has a weaker coordination to N1, comparing to the other nitrogen atoms.[24] Substitution of one bromide anion by a DMF solvent molecule increases this value from 5.6 to 17.0 kcal·mol^{-1} (**4** in comparison to **4a**). Another possibility would be that the bulky bromide anion pulls the metal away from the acridine ring nitrogen atom.

Table 3: NBO second-order perturbation theory analysis of the metal ion (Zn/Cd) coordination to **3** at the B3LYP-D3/def2-TZVPP level of theory.

$E^{(PT2)}$ [kcal·mol^{-1}]	N1	N2	N3
[(dmf)ZnBr{$(Me_2NCH_2)_2Acr$}]$^+$ (**4a**)	17.0	25.4	25.1
[$ZnBr_2${$(Me_2NCH_2)_2Acr$}] (**4**)	5.6	24.7	25.4
[$CdBr_2${$(Me_2NCH_2)_2Acr$}] (**5**)	4.7	22.8	22.7
[$(MeOH)_2Zn${$(Me_2NCH_2)_2Acr$}]$^{2+}$ (in MeOH)	21.9	25.4	26.5
[$(MeOH)_2Cd${$(Me_2NCH_2)_2Acr$}]$^{2+}$ (in MeOH)	15.0	32.1	31.8

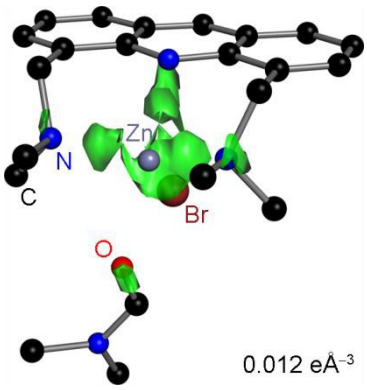

Figure 7: Computed difference electron density map of **4a** at an isosurface level of 0.012 eÅ^{-3}.

The NPA charges for the two compounds are 1.49 (**4**) and 1.60 (**4a**), so that the charge difference is not very significant. The second possibility, hence the interaction with a second bromide to weaken the coordination to the acridine seems to be the most likely explanation for this effect. Furthermore, we conducted calculations on the hypothetical complexes formed in solution, [$(MeOH)_2Zn${$(Me_2NCH_2)_2Acr$}]$^{2+}$ and [$(MeOH)_2Cd${$(Me_2NCH_2)_2Acr$}]$^{2+}$. Since we are interested to replicate the conditions in solution as close as possible the COSMO continuum model[25] was applied (for standard methanol solution conditions). The NBO results show that the coordination to the acridine nitrogen is strengthened (21.9 and 15.0 kcal·mol^{-1} for Zn^{2+} and Cd^{2+}, respectively). This is in line with the observations made when comparing **4** and **4a**. The complexes formed in the solid state have a weaker binding to the acridine moiety due to the crystallization with bromide anions. Our computed structures show smaller N1–Zn/Cd distances in agreement with this observation. The values are 216 and 237 pm, for Zn^{2+} and Cd^{2+} respectively. In methanol solution, sizeable interactions between the metal ion and the N1 nitrogen atom can be confirmed. The interactions with the side arm nitrogens are relatively constant, just slightly enhanced in solution. In Figure 7, the computed difference electron density map of **4a** is illustrated. The electron densities of the individual parts (**3**, Zn^{2+}, Br^-, and DMF) were computed and subtracted from the electron density of **4a**; all with the same geometry. This facilitates us to illustrate the regions where the electron density is enhanced due to the interaction of the relevant atoms.

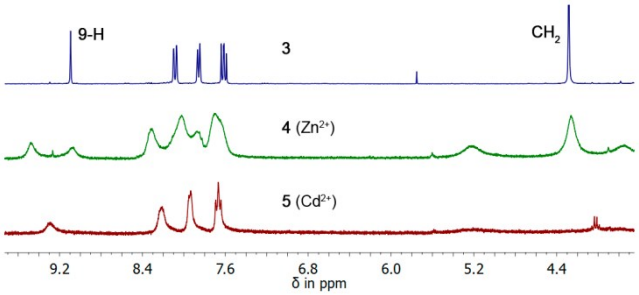

Figure 8: ^{1}H NMR spectra of compounds **3**–**5** in DMSO-d_6 at ambient temperature.

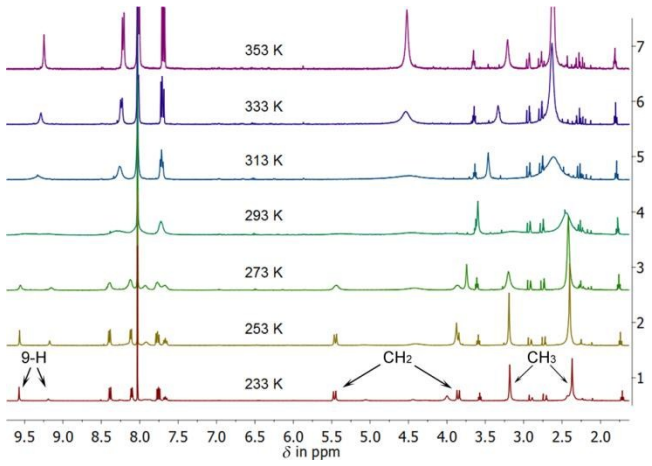

Figure 9: Temperature-dependent ^{1}H NMR spectra of **4** in DMF-d_7. The discussed signals are marked at 233 K.

The green cloud represents the accumulated electron density. Here, the interaction of the lone pairs of all three nitrogen atoms with the metal ion is accentuated. When comparing the results of the computational studies with the fluorescence properties, it is apparent that the emission wavelength does not change significantly by adding the metal salts to the sensor solutions, although the aromatic system is involved in the complexation of the metal ions. A possible explanation would be that the coordination does not influence the π-system significantly. Considering the geometry optimisations for the complex in methanol solution, both metal ion interactions with the aromatic nitrogen atom become stronger.

This should also be the case for the titration experiment of the fluorescence measurements. For a deeper insight into the liquid phase, we recorded several ^{1}H NMR spectra depicted in Figure 8. In comparison to the spectrum of the pure ligand, the complexes show significantly broadened signals. This is often caused by dynamic processes. Consequently we measured the spectrum of **4** at different temperatures (Figure 9). Increase of the temperature sharpens the broad signals until one definite set of signals is obtained (353 K). At lower temperatures, the spectrum splits into two different sets of signals with a maximum intensity at around 253 K. At this temperature they exhibit an intensity ratio of around 2:1 which can be monitored by the singlet of the H-9 proton at 9.57 ppm and 9.17 ppm, respectively. This splitting is most likely to be attributed to the exchange of the bromine atoms with the solvent DMF. To prove this statement, we carried out a pseudo 2D ^{1}H DOSY experiment at low temperature and added an excess of NaBr to the NMR sample. After the addition, a third set of signals appears whereby the intensity ratio of the other two sets of signals is reversed (SI Figure S3.13). The diffusion coefficient of the rising signals decreases slightly which can be explained by the smaller radius/mass ratio of a bromine atom compared to a DMF molecule.[26] Consequently, the latter should represent the dibrominated species (**4**). The new signals have a diffusion coefficient which lies between the two others and are therefore assigned to the monobrominated compound (**4a**). Furthermore, the signals at room temperature are no longer broadened after the addition of NaBr. That is why the dynamic processes can be attributed to this solvent/bromide exchange.

At the coalescence temperature of nearly 303 K, the diastereotopicity of the CH_2 protons becomes visible. The signal of the four methyl groups at the amines splits into two signals. The velocity of their hindered rotation caused by the coordination of the zinc ion lies underneath the NMR timescale at lower temperatures and can be monitored. Zinc ions are spectroscopically silent which makes it difficult to detect a ligand-metal interaction by NMR spectroscopy. However, we measured the ^{15}N NMR chemical shifts of the free ligand and of the zinc complex. The comparison of the resulting shifts shows a small but significant deshielding of $\Delta\delta$ = 8.6 ppm.[27]

In principle, the ^{1}H NMR spectra of **5** show similar dependencies upon temperature variation (SI Figure S3.17). The coalescence temperature in DMF-d_7 is around 313 K where the diastereotopicity of the CH_2 protons becomes visible as well as the mentioned splitting of the signal of the methyl groups. But in this case no second set of signals appears and the spectrum is less broadened. The advantage of this complex is the NMR active ^{113}Cd nucleus. Employing a 2D ^{113}Cd,^{1}H-HMBC experiment at low temperature, we could identify vicinal couplings of the methyl and methylene protons to the metal ion (SI Figure S3.18). The chemical shift of the cadmium isotope is –345 ppm, referenced to Me_2Cd. Interestingly, a coupling to the ^{113}Cd nucleus was only observed for one proton of each methylene group. The coupling to the other proton is likely not to be observed due to an unfavourable angle between the related atoms.[28] From the NMR spectroscopic experiments it is clear that the complexes adopt the same contact ion pairs in solution as observed in the solid state. Another analytical method which allows investigating the transferability of the solid state structure to solution is mass spectrometry. We chose a time-of-flight (TOF) spectrometer in combination with the mild electrospray ionisation method because of the poor solubility in most of the

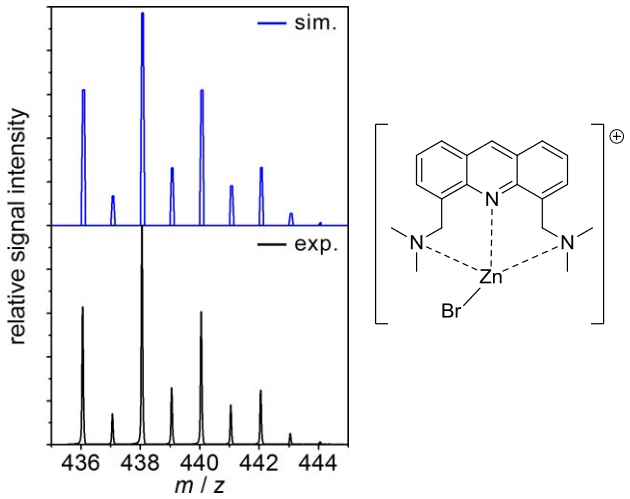

Figure 10: Extract from the mass spectrum of the cationic **4**, showing the simulated (blue) and the experimental (black) isotope pattern of the positive charged complex.

common solvents (e.g. THF, MeOH, MeCN). The measurements were performed in pure THF for the zinc complex and in THF/H_2O for the cadmium complex due to the even lower solubility. However, both complexes were sufficiently present in solution for the TOF spectrometer. Figure 10 depicts a comparison of two mass patterns. The black lines represent the experimental data from the zinc complex, whereas the blue lines illustrate the simulated spectrum for the proposed structural motif (in the positive ion mode one bromide anion was omitted for the calculated spectrum). The comparison demonstrates a perfect match of the predicted and observed species. Furthermore, the full mass spectrum is free of any ionic fragments because only signals generated by the acridine derivative, with and without metal ion, and related fragments can be detected. The same is valid for the Cd^{2+} complex (SI Figure S6.5). Both methods, NMR spectroscopy and mass spectrometry, emphasize that the solid state structure is maintained in solution. As mentioned in the introduction, molecular sensors play a key role in a wide range of areas, especially in medicinal or analytical applications. In this publication, we have mainly shown the possibility to use our sensor molecules in very polar solvents (fluorescence measurements in MeOH; NMR in DMF; ESI-MS in THF). However, using water as a solvent frequently evokes serious challenges. Despite the poor solubility of organic molecules, the self-ionization of water mainly results in the protonation of the amine side-arm receptor units. This dramatically hampers the coordination of analytes. Additionally, the pK_a value of acridine rises from 5.45 to 10.7 when getting excited in the fluorescence spectrometer,[29] an even higher value than the aliphatic amine (~9.7, value of the related *N*,*N*-dimethylbenzylamine).[30] The formation of the protonated species can easily be monitored by fluorescence and NMR spectroscopy. In the laboratory, the addition of hydrochloric acid to a clear solution of **3** in toluene resulted in a yellow precipitate. The solubility in this solvent is reduced due to the induced charge in the product. After purification, a ^{1}H NMR spectrum in DMSO-d_6 shows the attached proton and the related coupling constants. Furthermore, the solid state crystal structure of this salt could be determined (SI Figures S3.19 and S7.2). With **2**, the protonation experiment was not feasible. On account of the aniline like structure, the lone pair of the nitrogen atom is partly delocalized in the phenyl ring which results in a lower basicity (+M effect).[31]

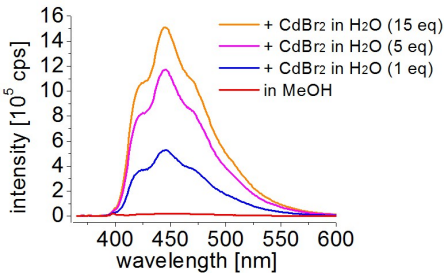

Figure 11: Emission spectra of **3** in methanol for various concentrations of $CdBr_2$ dissolved in purified water (λ_{exc} = 357 nm).

To achieve an enhancement of the emission intensity, a large excess of hydrochloric acid was needed, whereas for **3**, already two equivalents of the acid resulted in a notable change of the spectrum (SI Figure S5.3-4). The latter was expected for this compound since with regard to the lone pair the bonding to a proton is equivalent to the coordination of a metal ion. In both cases the PET is quenched and the emission of light is facilitated. According to these results, measurements in water were only reasonable with a buffer system in a high pH region (> 11). However, we could prevent these difficulties by solving the ligand in methanol and the analyte in water. In Figure 11, the good sensitivity of the sensor system towards Cd^{2+} ions is still present even in the presence of water.

Conclusions

The fluorescence spectra of ligand **3** show a remarkable metal ion selectivity and increase in fluorescence emission upon titration with dissolved $ZnBr_2$ and $CdBr_2$ in methanol/water. We could demonstrate the high sensitivity of the acridine based sensor molecule and the good stability of the systems. The solid state contact ion pairs **4** and **5** determined by X-ray structure analyses were confirmed to be present both in the gas phase by computational chemistry and in solution by NMR spectroscopy and mass spectrometry. This features the 4,5-bis(*N*,*N*-dimethylaminemethylene)acridine a valuable ligand in the medical and environmental important photochemical detection of zinc and cadmium ions. Compared to the numerous publications concerning zinc sensors, only very few provide structural evidence of the metal ion coordination, although this is inevitable for the accurate understanding of fluorescence processes.

Experimental Section

Materials and Measurements

All materials were purchased from SIGMA-ALDRICH, VWR INTERNATIONAL, and ABCR CHEMICALS and used without further purification – except water which was purified first through a Millipore water purification system Milli-RO 3 plus and finally with a Millipore ultrapure water system Milli-Q plus 185. The NMR measurements were performed on a BRUKER Avance III 300 and BRUKER Avance III HD 400 spectrometer. The chemical shifts (δ) are reported in parts per milion (ppm) relative to the residual proton signals of the incompletely deuterated solvents. The fluorescence measurements were carried out on a HORIBA JOBIN-YVON Fluoromax-4 spectrometer. All emission spectra were recorded with an excitation wavelength of 357 nm. For eletrospray ionization mass spectrometric studies, sample solutions of $c \approx 5$ mm were continuously administered into the ESI source of a micrOTOF-Q II mass spectrometer (BRUKER DALTONIK) by a step motor-driven gas-tight syringe (flow rate: 0.5 ml/h). This instrument combines a quadrupole mass filter with a time-of-flight analyzer. The simulated isotope patterns were calculated using the COMPASS® software package from BRUKER DALTONIK.

Single-Crystal Structural Analysis

Suitable single crystals for X-ray structural analysis were selected from a Schlenk flask under an argon atmosphere and covered with perfluorated polyether oil on a microscope slide, which was cooled with a nitrogen gas flow using the X-TEMP2 device.[32] An appropriate crystal was selected using a polarizing microscope, mounted on the tip of a MiTeGen MicroMount, fixed to a goniometer head and shock-cooled by the crystal cooling device. The data for **4a** were collected on an INCOATEC Mo microsource[33] with mirror optics and a Mo-K_α radiation with $\lambda = 71.073$ pm. The data for **5** were collected at an INCOATEC Ag microfocus source with INCOATEC Quazar mirror optics and an Ag radiation with $\lambda = 56.086$ pm. Both diffractometers were equipped with an APEX II detector with a D8 goniometer and a low-temperature device. The data for **4a** and **5** were integrated with SAINT[34] and an empirical absorption correction (SADABS)[35] was applied. The structures were solved by direct methods using SHELXT[36] and refined by full-matrix least-squares methods against F^2 (SHELXL)[37] within the SHELXLE GUI.[38] The hydrogen atoms were refined isotropically on calculated positions using a riding model with their U_{iso} values constrained to equal 1.5 times the U_{eq} of their pivot atoms for terminal sp^3 carbon atoms and 1.2 times for all other carbon atoms. Disordered moieties were refined using bond length restraints and anisotropic displacement parameter restraints.[39] Crystallographic data for the structures reported in this paper have been deposited within the Cambridge Crystallographic Data Centre. The CCDC numbers, crystal data, and experimental details for the X-ray measurements are listed in Table S7.2 of the SI. Copies of the data can be obtained free of charge from the Cambridge Crystallographic Data Centre via www.ccdc.cam.ac.uk/data_request/cif or from the corresponding author.

Computational studies

All geometry optimizations were carried out at the B3LYP-D3/def2-TZVPP[21, 40] level of theory (including Becke-Jones type damping[41] of the dispersion correction[21f]). In the case of Cd, the Stuttgart/Dresden ECP28MDF[42] was used. The electronic densities and the corresponding NBO analysis[22-23] were computed at the same level. All calculations were carried out with the ORCA[43] program package. The B3LYP calculations were performed under the RIJCOSX approximation[44].

Synthesis of 4,5-bis(bromomethylene)acridine (1): A solution of acridine (4.06 g, 22.6 mmol, 1.0 eq) in conc. H_2SO_4 (50 ml) was heated up to 50 °C when BMME (7.4 ml, 90.6 mmol, 4.0 eq) was added. After stirring for 17 h at this temperature the reaction mixture was cooled to rt and the formed excess of bromine gas was discharged through an aqueous solution of thiosulfate. The crude product precipitated by pouring into ice (400 g) and stirring for 1 h. The yellow precipitate was filtered, washed several times with dem. water and dissolved in chloroform (400 ml). The solution was washed with brine (3x 200 ml) and the gathered aqueous phases were extracted with chloroform (100 ml). The organic phases were dried with $MgSO_4$, filtered and the solvent was removed under reduced pressure. For purification, the crude dark yellow product was recrystallized from chloroform two times to obtain a light yellow powder (2.54 g, 6.96 mmol, 30.7%). ^{1}H NMR (300 MHz, $CDCl_3$): δ 8.78 (s, 1 H, H_9), 7.99 (d, ^3J = 8.5 Hz, 2 H, $H_{1,8}$), 7.94 (d, ^3J = 6.8 Hz, 2 H, $H_{3,6}$), 7.51 (dd, ^3J = 8.5 Hz, 6.9 Hz, 2 H, $H_{2,7}$), 5.43 (s, 4 H, CH_2). ^{13}C{^{1}H} NMR (75.5 MHz, $CDCl_3$): δ 145.8 (2 C, $C_{4a,10a}$), 136.8 (1 C, C_9), 136.5 (2 C, $C_{4,5}$), 131.3 (2 C, $C_{3,6}$), 129.2 (2 C, $C_{1,8}$), 126.9 (2 C, $C_{8a,9a}$), 126.0 (2 C, $C_{2,7}$), 30.3 (2 C, CH_2). EI-MS: *m/z* (%) 365 (34) $[M]^{+\bullet}$, 286/284 (76/76) $[M–Br]^{+\bullet}$, 205 (100) $[M–Br_2]^{+\bullet}$. Anal. Calcd for $C_{15}H_{11}Br_2N$: C, 49.35; H, 3.04; N, 3.84; Br, 43.78. Found: C, 48.86; H, 3.06; N, 3.78; Br, 43.30.

Synthesis of 4,5-bis(*N*-methyl-*N*-phenylaminemethylene)-acridine (2): To a suspension of **1** (0.50 g, 1.37 mmol, 1.0 eq) and K_2CO_3 (0.66 g, 4.78 mmol, 3.5 eq) in MeCN (30 ml) methylphenylamine (0.30 ml, 2.76 mmol, 2.0 eq) was added. After stirring the reaction mixture for 4 h at rt, the volatile components were removed under reduced pressure. The crude product was dissolved in ethyl acetate and aqueous NaCl solution and washed three times with brine. The organic layer was dried over $MgSO_4$, filtrated and the solvent was removed *in vacuo*. For further purification, a recrystallization from methanol was implemented. Thereby, the impurities were dissolved and filtrated off. **2** (0.49 mg, 1.17 mmol, 85.4%) could be obtained as a yellow solid. ^{1}H NMR (300 MHz, DMSO-d_6): δ 9.15 (s, 1 H, H_9), 8.07 (d, ^3J = 8.0 Hz, 2 H, $H_{1,8}$), 7.55 (dd, ^3J = 8.0 Hz, ^3J = 6.9 Hz, 2 H, $H_{2,7}$), 7.47 (d, ^3J = 6.9 Hz, 2 H, $H_{3,6}$), 7.12 (dd, ^3J = 8.6 Hz, ^3J = 7.2 Hz, 4 H, *meta*H_{Ph}), 6.73 (d, ^3J = 8.6 Hz, 4 H, *ortho*H_{Ph}), 6.58 (dd, ^3J = 7.2 Hz, ^3J = 7.2 Hz, 2 H, *para*H_{Ph}), 5.38 (s, 4 H, CH_2), 3.19 (s, 6 H, CH_3). ^{13}C{^{1}H} NMR (75.5 MHz, DMSO-d_6): δ 149.2 (2 C, *ipso*C_{Ph}), 145.8 (2 C, $C_{4a,10a}$), 136.7 (1 C, C_9), 135.7 (2 C, $C_{4,5}$), 129.0 (4 C, *meta*C_{Ph}), 127.0 (2 C, $C_{1,8}$), 126.8 (2 C, $C_{3,6}$), 126.1 (2 C, $C_{8a,9a}$), 125.6 (2 C, $C_{2,7}$), 115.6 (2 C, *para*C_{Ph}), 111.7 (4 C, *ortho*C_{Ph}), 52.6 (2 C, CH_2), 38.9 (2 C, CH_3). EI-MS: *m/z* (%) 417.2 (14) $[M]^{+\bullet}$, 310.1 (100) $[M–NMePh]^{+\bullet}$, 205.1 (84) $[M–(NMePh)_2]^{+\bullet}$. Anal. Calcd for $C_{29}H_{27}N_3$: C, 83.42; H, 6.52; N, 10.06. Found: C, 82.31; H, 6.33; N, 9.92.

Synthesis of 4,5-bis(*N*,*N*-dimethylaminemethylene)acridine (3): The synthesis procedure for **3** is the same as for **2**; with **1** (1.55 g, 4.25 mmol, 1.0 eq), K_2CO_3 (1.76 g, 12.75 mmol, 3.0 eq), a solution of dimethylamine in THF (2.0 m, 4.5 ml, 9.0 mmol, 2.1 eq), and MeCN (40 ml). The desired product (0.78 g, 2.66 mmol, 62.6%) could be obtained as a yellow-brown solid. ^{1}H NMR (300 MHz, DMSO-d_6): δ 9.09 (s, 1 H, H_9), 8.08 (dd, ^3J = 8.5 Hz, ^4J = 1.6 Hz, 2 H, $H_{1,8}$), 7.86 (dd, ^3J = 6.8 Hz, ^4J = 1.3 Hz, 2 H, $H_{3,6}$), 7.61 (dd, ^3J = 8.5, 6.8 Hz, 2 H, $H_{2,7}$), 4.28 (s, 4 H, CH_2), 2.35 (s, 12 H, CH_3). ^{13}C{^{1}H} NMR (75.5 MHz, DMSO-d_6): δ 146.2 (2 C, $C_{4a,10a}$), 136.6 (2 C, $C_{4,5}$), 135.9 (1 C, C_9), 130.0 (2 C, $C_{3,6}$), 127.4 (2 C, $C_{1,8}$), 125.9 (2 C, $C_{8a,9a}$), 125.6 (2 C, $C_{2,7}$), 58.2 (2 C, CH_2), 45.4 (4 C, CH_3). ^{15}N-HMBC (40.6 MHz, DMF-d_7): δ –81.2 (N_{arom}), –355.3 (NMe_2). EI-MS: *m/z* (%) 293 (4) $[M]^{+\bullet}$, 250 (64) $[M–NMe_2]^{+\bullet}$, 205 (100) $[M–(NMe_2)_2]^{+\bullet}$. Anal. Calcd for $C_{19}H_{23}N_3$: C, 77.78; H, 7.90; N, 14.32. Found: C, 76.45; H, 7.77; N, 13.94.

Synthesis of 4,5-bis(*N*,*N*-dimethylaminemethylene)acridine dibromido zinc(II) (4): 2 (175 mg, 596 µmol, 1.0 eq) was

dissolved in THF (1 ml) and a solution of $ZnBr_2$ (134 mg, 596 µmol, 1 eq) in THF (0.2 ml) was added dropwise. Thereby, the zinc complex precipitated immediately. The suspension was filtrated and washed several times with THF. The zinc complex (145 mg, 280 µmol, 47.0%) was isolated as a yellow powder. Suitable crystals for X-ray analysis could be grown after recrystallization from a THF/DMF (9:1) mixture. The crystals were formed at rt after two weeks. ^{1}H NMR (400 MHz, DMF-d_7, 353 K): δ 9.25 (s, 1 H, H_9), 8.22 (d, ^3J = 8.3 Hz, 2 H, $H_{1,8}$), 8.01 (d, ^3J = 7.1 Hz, 2 H, $H_{3,6}$), 7.69 (dd, ^3J = 8.3, 7.1 Hz, 2 H, $H_{2,7}$), 4.52 (4 H, CH_2), 2.62 (s, 12 H, CH_3). ^{13}C{^{1}H} NMR (100 MHz, DMF-d_7, 243 K): δ 148.7 (2 C, $C_{4a,10a}$), 142.0 (1 C, C_9), 135.5 (2 C, $C_{3,6}$), 130.5 (2 C, $C_{1,8}$), 127.7 (2 C, $C_{8a,9a}$), 126.4 (2 C, $C_{2,7}$), 63.1 (2 C, CH_2), 48.9 (2 C, CH_3), 46.4 (2 C, CH_3). ^{15}N NMR (40.6 MHz, DMF-d_7, 243 K): δ –346.7 (NMe_2). ESI-TOF: *m/z*: 813.15 $[(C_{19}H_{23}N_3)_2ZnBr_2H]^+$, 438.05 $[(C_{19}H_{23}N_3)ZnBr]^+$, 294.20 $[(C_{19}H_{23}N_3)H]^+$. Anal. Calcd for $C_{19}H_{23}N_3ZnBr_2$: C, 44.00; H, 4.47; N, 8.10; Br, 30.81. Found: C, 44.00; H, 4.50; N, 8.10; Br, 30.00.

Synthesis of 4,5-bis(*N*,*N*-dimethylaminemethylene)acridine dibromido cadmium(II) (5): 2 (141 mg, 480 µmol, 1.0 eq) was dissolved in methanol (0.5 ml) and a solution of $CdBr_2$ (131 mg, 480 µmol, 1.0 eq) in methanol (1.5 ml) was poured into. Upon addition, the cadmium complex precipitated immediately. Another 5 ml of methanol were added and the suspension was filtered. The residue was washed several times with methanol (3x 5 ml) and dried under reduced pressure. The pure product (245 mg, 433 µmol, 90.2%) was obtained as a yellow powder. The product was dissolved in a THF/DMF (3:2) mixture, heated up to the boiling point of THF and then cooled to rt overnight. The crystals thus formed were suitable for X-ray diffraction. ^{1}H NMR (400 MHz, DMF-d_7, 353 K): δ 9.32 (s, 1 H, H_9), 8.28 (d, ^3J = 8.5 Hz, 2 H, $H_{1,8}$), 8.08-7.99 (m, 2 H, $H_{3,6}$), 7.71 (dd, ^3J = 8.5, 6.8 Hz, 2 H, $H_{2,7}$), 4.56 (s, 4 H, CH_2), 2.74 (s, 12 H, CH_3). ^{113}Cd,^{1}H-HMBC (66.6 MHz, DMF-d_7, 243 K): δ –345.5. ESI-TOF: *m/z*: 861.15 $[(C_{19}H_{23}N_3)_2CdBr_2H]^+$, 486.02 $[(C_{19}H_{23}N_3)CdBr]^+$, 294.21 $[(C_{19}H_{23}N_3)H]^+$. Anal. Calcd for $C_{19}H_{23}N_3CdBr_2$: C, 40.35; H, 4.10; N, 7.43; Cd, 19.87. Found: C, 40.28; H, 4.31; N, 7.20; Cd, 19.00.

Acknowledgements

Thanks to the Danish National Research Foundation (DNRF93) funded *Center for Materials Crystallography* (CMC) for partial support and the Land Niedersachsen for providing a fellowship in the GAUSS PhD program. We also want to thank Timo Schillmöller for the support of some fluorescence measurements.

Notes and references

1 (a) W. N. Lipscomb and N. Sträter, *Chem. Rev.*, 1996, **96**, 2375-2434; (b) R. McRae, P. Bagchi, S. Sumalekshmy and C. J. Fahrni, *Chem. Rev.*, 2009, **109**, 4780-4827.

2 (a) J.-Y. Koh, S. W. Suh, B. J. Gwag, Y. Y. He, C. Y. Hsu and D. W. Choi, *Science*, 1996, **272**, 1013-1016; (b) A. I. Bush, *Curr. Opin. Chem. Biol.*, 2000, **4**, 184-191.

3 (a) M. Cortesi, E. Fridman, A. Volkov, S. S. Shilstein, R. Chechik, A. Breskin, D. Vartsky, N. Kleinman, G. Kogan, E. Moriel, V. Gladysh, M. Huszar, J. Ramon and G. Raviv, *The Prostate*, 2008, **68**, 994-1006; (b) Z. Medarova, S. K. Ghosh, M. Vangel, R. Drake and A. Moore, *Am. J. Cancer Res.*, 2014, **4**, 385-393.

4 (a) J. M. Berg and Y. Shi, *Science*, 1996, **271**, 1081-1085; (b) N. Wellinghausen, M. Martin and L. Rink, *Eur. J. Immunol.*, 1997, **27**, 2529-2535; (c) M. J. Salgueiro, M. Zubillaga, A. Lysionek, M. I. Sarabia, R. Caro, T. De Paoli, A. Hager, R. Weill and J. Boccio, *Nutr. Res.*, 2000, **20**, 737-755.

5 (a) K. Nogawa, A. Ishizaki and E. Kobayashi, *Environ. Res.*, 1979, **18**, 397-409; (b) C. Tohyama, Z. A. Shaikh, K. Nogawa, E. Kobayashi and R. Honda, *Arch. Toxicol.*, 1982, **50**, 159-166.

6 Y. Li, T. Liu, H. Liu, M.-Z. Tian and Y. Li, *Acc. Chem. Res.*, 2014, **47**, 1186-1198.

7 T. Saha, A. Sengupta, P. Hazra and P. Talukdar, *Photochem. Photobiol. Sci.*, 2014, **13**, 1427-1433.

8 J. B. Briks, *Photophysics of Aromatic Molecules*, Wiley - Interscience, London, New York, Sydney, Toronto, 1st edn., 1970.

9 (a) R. A. Bissel, A. P. de Silva, H. Q. N. Gunaratne, P. L. M. Lynch, G. E. M. Maguire, C. P. McCoy and K. R. A. S. Sandanayake, in *Photoinduced Electron Transfer V*, ed. J. Mattay, Springer, Berlin, Heidelberg, 1993, vol. 168, pp. 229-230; (b) K. Kubo, in *Topics in Fluorescence Spectroscopy*, ed. C. D. Geddes and J. R. Lakowicz, Springer US, 2005, vol. 9, ch. 6, pp. 219-247; (c) A. P. de Silva, *J. Phys. Chem. Lett.*, 2011, **2**, 2865-2871.

10 (a) A. P. de Silva, H. Q. N. Gunaratne, T. Gunnlaugsson, A. J. M. Huxley, C. P. McCoy, J. T. Rademacher and T. E. Rice, *Chem. Rev.*, 1997, **97**, 1515-1566; (b) Z. Fei, N. Kocher, C. J. Mohrschladt, H. Ihmels and D. Stalke, *Angew. Chem. Int. Ed.*, 2003, **42**, 783-787; *Angew. Chem.* 2003, **115**, 807-811; (c) A. Ajayaghosh, P. Carol and S. Sreejith, *J. Am. Chem. Soc.*, 2005, **127**, 14962-14963; (d) K. Ono, J. K. Klosterman, M. Yoshizawa, K. Sekiguchi, T. Tahara and M. Fujita, *J. Am. Chem. Soc.*, 2009, **131**, 12526-12527; (e) Z. Xu, J. Yoon and D. R. Spring, *Chem. Soc. Rev.*, 2010, **39**, 1996-2006; (f) H. Woo, S. Cho, Y. Han, W.-S. Chae, D.-R. Ahn, Y. You and W. Nam, *J. Am. Chem. Soc.*, 2013, **135**, 4771-4787; (g) M. Yamashina, M. M. Sartin, Y. Sei, M. Akita, S. Takeuchi, T. Tahara and M. Yoshizawa, *J. Am. Chem. Soc.*, 2015, **137**, 9266-9269.

11 (a) J. Joseph, E. Kuruvilla, A. T. Achuthan, D. Ramaiah and G. B. Schuster, *Bioconjugate Chem.*, 2004, **15**, 1230-1235; (b) Z. Ma, J. R. Choudhury, M. W. Wright, C. S. Day, G. Saluta, G. L. Kucera and U. Bierbach, *J. Med. Chem.*, 2008, **51**, 7574-7580.

12 (a) H. N. Lee, H. N. Kim, K. M. K. Swamy, M. S. Park, J. Kim, H. Lee, K.-H. Lee, S. Park and J. Yoon, *Tetrahedron Lett.*, 2008, **49**, 1261-1265; (b) J. Kertész, B. Bognár, A. Kormos, I. Móczár, P. Baranyai, M. Kubinyi, T. Kálai, K. Hideg and P. Huszthy, *Tetrahedron*, 2011, **67**, 8860-8864.

13 M. S. Park, K. M. K. Swamy, Y. J. Lee, H. N. Lee, Y. J. Jang, Y. H. Moon and J. Yoon, *Tetrahedron Lett.*, 2006, **47**, 8129-8132.

14 (a) S. Cao, H. Li, T. Chen and J. Chen, *J. Solution Chem.*, 2009, **38**, 1520-1527; (b) E. B. Veale and T. Gunnlaugsson, *Annu. Rep. Prog. Chem., Sect. B*, 2010, **106**, 376-406.

15 J. Chiron and J.-P. Galy, *Synlett*, 2003, **15**, 2349-2350.

16 M. E. Huston, K. W. Haider and A. W. Czarnik, *J. Am. Chem. Soc.*, 1988, **110**, 4460-4462.

17 J. F. Mammone, S. K. Sharma and M. Nicol, *J. Phys. Chem.*, 1980, **84**, 3130-3134.

18 (a) C. Gunanathan, L. J. W. Shimon and D. Milstein, *J. Am. Chem. Soc.*, 2009, **131**, 3146-3147; (b) X. Ye, P. N. Plessow, M. K.

Brinks, M. Schelwies, T. Schaub, F. Rominger, R. Paciello, M. Limbach and P. Hofmann, *J. Am. Chem. Soc.*, 2014, **136**, 5923-5929.
19 (a) F. H. Allen, *Acta Cryst. B*, 2002, **58**, 380-388; (b) Cambridge Structural Database, v5.36 (November 2014), Cambridge, UK, 2015.
20 U. Flierler and D. Stalke, in *Structure and Bonding*, ed. D. Stalke, Springer, Berlin, New York, 2012, vol. 146, pp. 1-20.
21 (a) A. D. Becke, *Phys. Rev. A*, 1988, **38**, 3098-3100; (b) C. Lee, W. Yang and R. G. Parr, *Phys. Rev. B*, 1988, **37**, 785-789; (c) A. D. Becke, *J. Chem. Phys.*, 1993, **98**, 5648-5652; (d) P. J. Stephens, F. J. Devlin, C. F. Chabalowski and M. J. Frisch, *J. Phys. Chem.*, 1994, **98**, 11623-11627; (e) F. Weigend and R. Ahlrichs, *Phys. Chem. Chem. Phys.*, 2005, **7**, 3297-3305; (f) S. Grimme, J. Antony, S. Ehrlich and H. Krieg, *J. Chem. Phys.*, 2010, **132**, 154104-154119.
22 (a) J. P. Foster and F. Weinhold, *J. Am. Chem. Soc.*, 1980, **102**, 7211-7218; (b) A. E. Reed, R. B. Weinstock and F. Weinhold, *J. Chem. Phys.*, 1985, **83**, 735-746; (c) E. D. Glendening, J. K. Badenhoop, A. E. Reed, J. E. Carpenter, J. A. Bohmann, C. M. Morales and F. Weinhold, *GenNBO 5.9*, University of Wisconsin, Madison, 2009.
23 A. E. Reed, L. A. Curtiss and F. Weinhold, *Chem. Rev.*, 1988, **88**, 899-926.
24 C. Maaß, D. M. Andrada, R. A. Mata, R. Herbst-Irmer and D. Stalke, *Inorg. Chem.*, 2013, **52**, 9539-9548.
25 A. Klamt and G. Schüürmann, *J. Chem. Soc., Perkin Trans. 2*, 1993, 799-805.
26 (a) A. Bondi, *J. Phys. Chem.*, 1964, **68**, 441-451; (b) R. Neufeld and D. Stalke, *Chem. Sci.*, 2015, **6**, 3354-3364.
27 (a) H. Gornitzka and D. Stalke, *Eur. J. Inorg. Chem.*, 1998, 311-317; (b) T. E. Wood, B. Berno, C. S. Beshara and A. Thompson, *J. Org. Chem.*, 2006, **71**, 2964-2971.
28 M. Karplus, *J. Am. Chem. Soc.*, 1963, **85**, 2870-2871.
29 J. R. Lakowicz and A. Balter, *Biophys. Chem.*, 1982, **16**, 117-132.
30 U. Knips and F. Huber, *Z. Naturforsch.*, 1983, **38b**, 434-436.
31 J. N. Murrell, *Proc. Phys. Soc. A*, 1955, **68**, 969-975.
32 (a) T. Kottke and D. Stalke, *J. Appl. Cryst.*, 1993, **26**, 615-619; (b) T. Kottke, R. J. Lagow and D. Stalke, *J. Appl. Cryst.*, 1996, **29**, 465-468; (c) D. Stalke, *Chem. Soc. Rev.*, 1998, **27**, 171-178.
33 T. Schulz, K. Meindl, D. Leusser, D. Stern, J. Graf, C. Michaelsen, M. Ruf, G. M. Sheldrick and D. Stalke, *J. Appl. Cryst.*, 2009, **42**, 885-891.
34 Bruker AXS Inc., SAINT v8.30C, Madison, WI, USA, 2013.
35 L. Krause, R. Herbst-Irmer, G. M. Sheldrick and D. Stalke, *J. Appl. Crystallogr.*, 2015, **48**, 3-10.
36 G. M. Sheldrick, *Acta Cryst. A*, 2015, **71**, 3-8.
37 G. M. Sheldrick, SHELXL in SHELXTL v2014/7, Madison, WI, USA, 2014.
38 C. B. Huebschle, G. M. Sheldrick and B. Dittrich, *J. Appl. Cryst.*, 2011, **44**, 1281-1284.
39 P. Müller, R. Herbst-Irmer, A. L. Spek, T. R. Schneider and M. R. Sawaya, *Crystal structure refinement - A crystallographer's guide to SHELXL*, Oxford University Press, Oxford, 8th edn., 2006.
40 K. Eichkorn, F. Weigend, O. Treutler and R. Ahlrichs, *Theor. Chem. Acc.*, 1997, **97**, 119-124.
41 (a) E. R. Johnson and A. D. Becke, *J. Chem. Phys.*, 2005, **123**, 024101; (b) A. D. Becke and E. R. Johnson, *J. Chem. Phys.*, 2005, **123**, 154101; (c) E. R. Johnson and A. D. Becke, *J. Chem. Phys.*, 2006, **124**, 174104.
42 D. Andrae, U. Häußermann, M. Dolg, H. Stoll and H. Preuß, *Theor. Chim. Acta*, 1990, **77**, 123-141.
43 F. Neese, *WIREs Comput. Mol. Sci.*, 2012, **2**, 73-78.
44 (a) E. J. Baerends, D. E. Ellis and P. Ros, *Chem. Phys.*, 1973, **2**, 41-51; (b) J. L. Whitten, *J. Chem. Phys.*, 1973, **58**, 4496-4501; (c) F. Neese, F. Wennmohs, A. Hansen and U. Becker, *Chem. Phys.*, 2009, **356**, 98-109.